

# Re-equilibration of natural H<sub>2</sub>O–CO<sub>2</sub>–salt-rich fluid inclusions in quartz—Part 1: experiments in pure water at constant pressures and differential pressures at 600 °C

Miriam Baumgartner · Ronald J. Bakker · Gerald Doppler

Received: 22 December 2013 / Accepted: 13 May 2014  
© European Union 2014

**Abstract** Re-equilibration processes of natural H<sub>2</sub>O–CO<sub>2</sub>–NaCl-rich fluid inclusions quartz are experimentally studied by exposing the samples to a pure H<sub>2</sub>O external fluid at 600 °C. Experimental conditions are selected at nearly constant pressure conditions (309 MPa) between fluid inclusions and pore fluid, with only fugacity gradients in H<sub>2</sub>O and CO<sub>2</sub>, and at differential pressure conditions (394–398 MPa, corresponding to an internal under-pressure) in addition to similar CO<sub>2</sub> fugacity gradients and larger H<sub>2</sub>O fugacity gradients. Modifications of fluid inclusion composition and density are monitored with changes in ice dissolution temperature, clathrate dissolution temperature and volume fraction of the vapour phase at room temperature. Specific modification of these parameters can be assigned to specific processes, such as preferential loss/gain of H<sub>2</sub>O and CO<sub>2</sub>, or changes in total volume. A combination of these parameters can clearly distinguish between modifications according to bulk diffusion or deformation processes. Bulk diffusion of CO<sub>2</sub> according to fugacity gradients is demonstrated at constant pressure conditions. The estimated preferential loss of H<sub>2</sub>O is not in accordance with those gradients in both constant pressure and differential pressure experiments. The development of deformation halos in quartz around fluid inclusions that are either under-pressurized or over-pressurized promotes

absorption of H<sub>2</sub>O from the inclusions and inhibits bulk diffusion according to the applied fugacity gradients.

**Keywords** Fluid inclusions · Re-equilibration experiments · Diffusion · H<sub>2</sub>O–CO<sub>2</sub>–NaCl · Quartz

## Introduction

Fluid inclusions may contain direct evidence of the conditions of geological environments in which they were trapped, as they are representative samples of specific hydrothermal fluids that were present during the formation and/or exhumation of rock. They are considered to be isolated “containers” in minerals, which do not interact with an external fluid, and therefore, density and composition after formation are assumed to remain constant. Experimental and field studies have shown that this assumption is occasionally incorrect and fluid inclusions do not always behave as closed systems (e.g. Bakker and Jansen 1990, 1994; Sterner and Bodnar 1989; Ayllon et al. 2003). Post-entrapment modifications, i.e. alteration in composition and density, after initial fluid trapping are induced by various re-equilibration processes. Fluid exchange in natural systems between inclusions and pore fluid is often discussed as a consequence of deformation (e.g. Wilkins and Barkas 1978; Barker 1995; Audet and Günther 1999; Krenn et al. 2008). Fluid inclusions are thereby strongly distorted, and changes in fluid properties are accompanied by morphological changes of the inclusions (dismemberment, limited volume increase or decrepitation), or diffusion may occur along dislocation lines or other crystal defect structures that are formed by deformation. In addition to stress-induced re-equilibrations, bulk diffusion is activated by compositional changes of the

Communicated by J. Hoefs.

**Electronic supplementary material** The online version of this article (doi:10.1007/s00410-014-1017-3) contains supplementary material, which is available to authorized users.

M. Baumgartner · R. J. Bakker (✉) · G. Doppler  
Resource Mineralogy, Department of Applied Geosciences and Geophysics, Montanuniversity Leoben, Leoben, Austria  
e-mail: bakker@unileoben.ac.at

external fluid (change of fugacity of fluid components) and/or by variances of external pressure and temperature conditions. In natural systems, a complex interaction of all those parameters may cause fluid inclusion alteration, whereas the major driving force of inclusion re-equilibration remains hidden. A great number of field studies (e.g. Ridley and Hagemann 1999; Ferrero et al. 2011; Faleiros et al. 2014) indicate that possible re-equilibration processes must be considered when fluid inclusions are used to interpret geological processes, like rock formation conditions. However, the interpretation of natural fluid inclusion alteration requires a detailed knowledge of the nature and celerity of fluid mass transport through a host mineral.

A variety of experimental re-equilibration studies with synthetic fluid inclusions have been carried out (Sternner and Bodnar 1989; Bakker and Jansen 1990, 1994; Sternner et al. 1995; Vityk and Bodnar 1995, 1998; Doppler et al. 2013), whereas experimental studies on natural inclusions are rare and incomplete. Schwab and Freisleben (1988) performed high-pressure experiments on natural CO<sub>2</sub>-rich inclusions in ultrabasic xenoliths, and they describe shrinkage and total fluid inclusion collapse as a consequence of increasing external pressure. Stress-induced alterations on natural fluid inclusions in quartz were also monitored by Vityk et al. (1994), Diamond et al. (2010) and Tarantola et al. (2010). Morphological features may imply modification on fluid inclusion properties, i.e. composition and molar volume. Re-equilibration textures caused by internal fluid over- and under-pressure were experimentally studied by Vityk et al. (1995) with natural hydrocarbon inclusions in quartz. In previous experimental studies, re-equilibration is caused by the effects of several driving forces applied at once (stress, temperature, pressure and fluid composition). Until now, fluid migration through a host mineral is not conclusive, as the impact of individual parameters, i.e. temperature, pressure, properties of the host mineral, fugacity gradients, and deformation processes, is not yet fully understood. A comprehensive knowledge of fluid transport mechanisms between an external fluid source (pore fluid) and fluid trapped in the host mineral can be gained only if the influence of each parameter can be distinguished.

The present experimental work first describes re-equilibration of natural H<sub>2</sub>O–CO<sub>2</sub>–NaCl-rich fluid inclusions under nearly constant pressure conditions, i.e. internal pressure ( $P_{\text{int}}$ ) in the inclusions is similar to the pressure of the external fluid ( $P_{\text{ext}}$ ). A gradient in fugacity between the pore fluid (pure H<sub>2</sub>O) and fluid inclusions is active and promotes isobaric fluid exchange mechanisms in the system of H<sub>2</sub>O–CO<sub>2</sub>–NaCl at experimental temperatures. The second part of this study involves a pure CO<sub>2</sub> pore fluid at similar temperature and pressure conditions and is presented in the follow-up manuscript (Bakker and

Baumgartner, in prep.). In addition, the experimental set-up is extended to  $\Delta P$  experiments, i.e. external pressure of the pore fluid is higher than internal fluid inclusion pressure ( $P_{\text{int}} < P_{\text{ext}}$ ). Therefore, the study provides individual observations of fluid inclusion alteration due to (1) a change in fugacity (i.e. chemical potential differences as the only driving force) and additionally due to (2) induced pressure gradients at high temperatures. Hydrothermal activities and fugacities of H<sub>2</sub>O, CO<sub>2</sub> and NaCl are calculated, and the newly acquired data illustrate a selective transport of the different components. The major driving forces responsible for fluid alteration after trapping are discussed, and the mobility of fluid components is regulated by a complex interaction of bulk diffusion and other processes such as microcrack enhanced or dislocation enhanced diffusion. The reliability of natural fluid inclusions for the determination of rock-forming conditions can be improved if re-equilibration processes are better understood.

## Methods

A proper investigation of the alteration of entrapped fluid due to re-equilibration requires a precise characterization of inclusions before and after experimentation. Natural H<sub>2</sub>O–CO<sub>2</sub>–NaCl-rich fluid inclusion assemblages, i.e. about sixty fluid inclusions in separated quartz slices, are individually studied and analysed by photomicrography to define details on inclusions shapes (perimeter, area and elongation), according to the method of Bakker and Diamond (2006). Relative total areas of liquid and vapour have been digitally measured from two-dimensional images by tracing the outside edge of the inclusion and the outside rim of the vapour bubble at room temperature. Relative modifications of the volume fractions of the vapour bubble are considered to correspond to relative modifications of area fractions. The position of each fluid inclusion in the quartz sample (three-dimensional distances from the quartz surface) is measured with an ordinary microscope with a stage that is adjustable in the  $x$ – $y$ – $z$ -direction (Olympus BX60). The shape parameters of each fluid inclusion are accurately measured before and after re-equilibration. Inclusions that reveal intensive leakage or refilling are not used for the general interpretation of diffusion and are discussed separately.

Microthermometry measurements were carried out with a LINKAM MDS 600 and LINKAM THMSG 600 heating–freezing stage. Calibration was done by using synthetic fluid inclusions with melting of CO<sub>2</sub> at –56.6 °C (triple point), melting of water at 0.0 °C (triple point) and the critical homogenization temperature of water at 374.0 °C. The instrument resolution of both stages is 0.1 °C, and the

standard deviation in each measurement is  $\pm 0.2$  °C in the range of  $-50$  to  $+50$  °C. The uncertainty analyses of these stages are given in detail in Doppler and Bakker (2014).

Additionally, Raman spectroscopic measurements have been used for the detection of fluid components and phase assemblage determination at low temperatures (down to  $-100$  °C; see also Baumgartner and Bakker 2010). Raman spectroscopy was performed with a LABRAM (ISA Jobin–Yvon) confocal spectrometer using a frequency-doubled 100-mW Nd-YAG laser with an excitation wavelength of  $\lambda = 532.6$  nm. All measurements were performed with an LMPlanFI 100x/0.80 (Olympus) objective lens.

Bulk fluid properties are determined by means of microthermometry in combination with Raman spectroscopy and volume fraction estimates for each inclusion. Total homogenization temperatures ( $T_h$ ) which are normally used in fluid inclusion studies to determine the bulk molar volume could not be detected as these natural inclusions decrepitate at temperatures above 230 °C, before homogenization was reached. As the dissolution temperatures of ice,  $T_m$  (ice), and clathrate,  $T_m$  (cla), are a direct function of  $V$ - $x$ -properties, initial fluid compositions and molar volumes have been calculated from these phase transition temperatures and estimated volume fractions with the computer program “ICE” and “CLATH” from the software package “CLATHRATES” (Bakker 1997), using the equation of state from Chueh and Prausnitz (1967) to calculate the fugacity of CO<sub>2</sub> at low temperatures and pressures in the presence of ice and clathrate. Clathrate stability in the H<sub>2</sub>O–CO<sub>2</sub>–NaCl fluid system was calculated according to the model of Bakker et al. (1996). Any shift in the dissolution points observed in the inclusions after re-equilibration can be directly related to compositional and density changes. For example, lowered ice dissolution temperatures (or freezing point depression) in binary H<sub>2</sub>O–NaCl-rich inclusions can be directly related to an increase in salinity, which is either a gain of NaCl or loss of H<sub>2</sub>O. In more complex systems (e.g. H<sub>2</sub>O–CO<sub>2</sub>–NaCl), any shift in the dissolution temperatures of salt hydrates, ice, clathrate and salts indicate compositional and density changes, though the exchange of components is not directly assignable because mass transfer of multiple components may occur. For example, diffusion of H<sub>2</sub>O into a H<sub>2</sub>O–CO<sub>2</sub>–NaCl-rich inclusion increases the dissolution temperatures of ice, whereas a coincidental gain of CO<sub>2</sub> has the reverse effect. Nevertheless, the divergence of phase transition temperatures before and after re-equilibration allows the re-calculation of fluid compositions in natural fluid inclusions according to specific processes if the thermodynamical properties of the fluid system are known. From the calculated initial fluid properties (composition and density), a stepwise theoretical preferential loss of H<sub>2</sub>O, preferential loss of CO<sub>2</sub> and total volume increase was used

to calculate the stepwise shift of ice and clathrate dissolution temperatures with the same software (Bakker 1997). Subsequently, changes in these temperatures of individual fluid inclusions can be directly related to one of these processes. In other words, the change in dissolution temperatures of ice and clathrate in the H<sub>2</sub>O–CO<sub>2</sub>–NaCl system is sensitive indicators of changes in the  $V$ - $x$  properties of fluid inclusions and do not depend on complicated procedures to calculate bulk mole fractions and density. The uncertainty in mole fraction exceeds vastly that of temperature measurements, because it depends on volume fraction estimations.

Re-equilibration experiments are performed in the hydrothermal laboratory at the Montanuniversity Leoben (see also Doppler et al. 2013). The experimental conditions were calculated from the estimated bulk properties of fluid inclusion (composition and density). Specific isochors for H<sub>2</sub>O–CO<sub>2</sub>–NaCl fluids at higher temperatures and pressures are calculated with the equation of state of Anderko and Pitzer (1993) and Duan et al. (1995), which can be directly applied with the software “ISOC” (Bakker 2003), or with newly developed software “Loner AP” (<http://fluids.unileoben.ac.at/>). This software is also used to calculate the fugacities of H<sub>2</sub>O, CO<sub>2</sub> and NaCl at experimental conditions. The fugacity of pure water is calculated with the equation of state of Haar et al. (1984) by using the software “Loner HGK” (<http://fluids.unileoben.ac.at/>).

## Source material

Regular and equant-shaped H<sub>2</sub>O–CO<sub>2</sub>–NaCl-bearing fluid inclusions of primary origin in quartz (Alpeiner Scharte, Tauern Window, Austria) were used for re-equilibration studies. Three doubly polished quartz discs (NI-002f, NI-001a and NI-002b) of about 3 mm in diameter and 0.6 mm in thickness were prepared (Fig. 1). The crystallographic orientation of the quartz cores was not exactly defined, due to the lack of crystallographic features of single quartz crystals (massive vein filling quartz).

Fluid inclusions are characterized by two phases at room temperature, i.e. NaCl-bearing aqueous solution and CO<sub>2</sub>-rich vapour bubble. Some natural inclusions contain ca. 1 μm sized of muscovite (identified with Raman spectroscopy) and/or an unknown opaque fibrous phase (possibly rutile). As not observed in all of the inclusions, these are considered accidentally trapped phases. Small calcite crystals (<1 μm) were also detected in some of the inclusions. Combined microthermometric and cryo-Raman spectroscopic observations reveal a phase assemblage of hydrohalite, ice and clathrate in the presence of vapour at low temperatures ( $-100$  °C). Hydrohalite completely dissolves at about  $-24.8$  to  $-22.3$  °C. Homogenization ( $T_h$ )

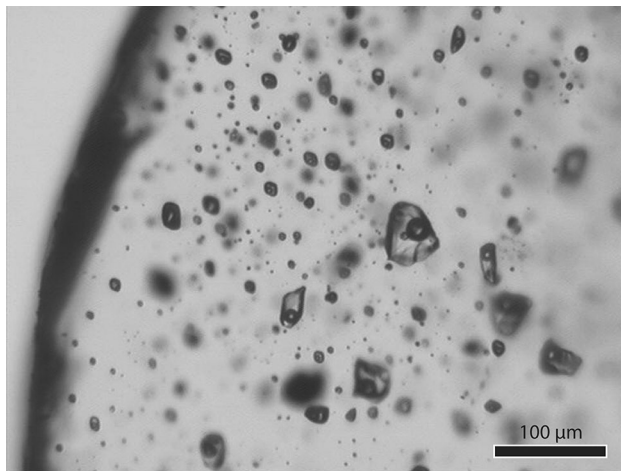


**Fig. 1** Photomicrograph of the original quartz disk with abundant natural fluid inclusions varying in size between 5 and 70  $\mu\text{m}$  in diameter, that is used in experiment *NI-002f*

of  $\text{CO}_2$  could not be observed as  $\text{CO}_2$  liquid, and vapour cannot be optically differentiated at low temperatures.

The primary obtained data, i.e. the range and mode of dissolution temperatures of ice and clathrate, and the volume fraction of the vapour phase in fluid inclusions in three quartz discs (*NI-002f*, *NI-001a*, and *NI-002b*) are given in

**Table 1** Range and mode values of ice and clathrate dissolution temperatures, i.e.  $T_m$  (ice) and  $T_m$  (cla), and volume fractions of the vapour phase ( $\phi^{\text{vap}}$ ) at room temperatures of inclusions in three different quartz discs (*Exp. no.*) that are used for re-equilibration

Exp. no.	<i>n</i>	$T_m$ (ice)		$T_m$ (cla)		$\phi^{\text{vap}}$		G.D.
		Range	Mode	Range	Mode	Range		
NI-002f	a	30	−8.0 to −7.4	−7.6	4.4–5.0	4.8	0.20–0.34	0.28 ± 0.04
	b	29	−7.4 to −6.0	−7.2	0.4–2.8	2.0	0.20–0.34	0.28 ± 0.02
NI-001a	58	7	−8.0 to −7.2	−7.4	4.8–5.6	5.0	0.20–0.38	0.30 ± 0.06
			−10.0 to −9.2	−9.4	4.8–5.6	4.8	0.18–0.34	0.26 <sup>a</sup>
NI-002b	58		−10.0 to −7.6	−9.2	4.2–5.8	5.2	0.22–0.40	0.31 ± 0.05

<sup>a</sup> Average of 7 measurements

**Table 2** Calculated range and average composition (mass %) of fluid inclusions and their molar volume ( $V_m$ ). Calculations are performed with the computer program “ICE” (Bakker 1997), using the equation

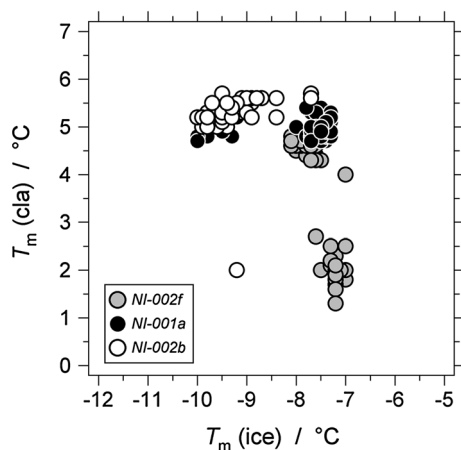
Exp. no.	<i>n</i>	Mass % $\text{H}_2\text{O}$		Mass % $\text{CO}_2$		Eq. mass % NaCl		$V_m$ in $\text{cm}^3 \text{mol}^{-1}$		
		Range	Average	Range	Average	Range	Average	Range	Average	
NI-002f	a	30	83.1–85.0	84.0	7.7–9.8	8.9	6.8–7.6	7.2	23.2–27.8	25.7
	b	29	85.2–86.8	85.9	5.7–7.4	6.8	6.9–7.7	7.3	23.2–27.9	25.6
NI-001a	58	7	83.0–85.3	84.0	7.6–10.8	9.2	6.3–7.5	6.8	23.2–29.5	26.2
			81.2–82.0	81.7	8.5–11.0	9.8	6.7–9.5	8.5	22.4–27.7	25.1
NI-002b	58		80.6–83.3	81.4	9.8–11.8	10.8	6.6–8.9	7.8	23.4–29.4	26.8

Table 1. The measurements of all individual fluid inclusions are given in the Supplementary material. The inclusions in sample *NI-002f*, *NI-001a*, and *NI-002b* are homogeneous assemblages with similar  $T_m$  (ice),  $T_m$  (cla) and  $\phi^{\text{vap}}$ . The calculated properties, i.e. average composition and molar volume (density) of fluid inclusions in each quartz disc, are given in Table 2. Again, the calculated properties of all individual fluid inclusions are given in the Supplementary material.

Despite the homogeneous character of inclusions in sample *NI-002f*, two groups with nearly equal dissolution temperatures of ice and clathrates can be distinguished (Fig. 2). One group showed a mode  $T_m$  (ice) of about  $-7.6$  °C and  $T_m$  (cla) of  $+4.8$  °C, whereas the other group revealed these temperatures at  $-7.2$  and  $+2.0$  °C, respectively (see Table 1). This minor variation emphasizes the homogeneity of this fluid inclusion assemblage. The calculated compositions of both groups are nearly equal (Table 2), with average values of 84.0 mass %  $\text{H}_2\text{O}$ , 8.9 mass %  $\text{CO}_2$  and 7.2 eq. mass % NaCl for the first group, whereas the other group has a similar salinity (7.3 eq. mass % NaCl), slightly depleted in  $\text{CO}_2$  (6.8 mass %) and relatively enriched in  $\text{H}_2\text{O}$  (85.9 mass %). According to the homogeneity in microthermometrical data and the similar appearance of all fluid inclusions in

experiments. The number of measured inclusions is given by *n*. G.D. is the centre and width of a Gaussian distribution curve that is fitted to volumetric data. A complete list of measurements of individual fluid inclusions is given in the Supplementary material

of state according to Chueh and Prausnitz (1967) to calculate the fugacity of vapour-like  $\text{CO}_2$  at  $T_m$  (ice) and  $T_m$  (cla)



**Fig. 2** Dissolution temperatures of ice,  $T_m(\text{ice})$  and clathrate,  $T_m(\text{cia})$  of the initial fluid inclusion assemblages in the experiments *NI-002f*, *NI-001a*, and *NI-002b*

photomicrographs, it is expected that all fluid inclusions have similar volume fractions of the vapour phase at room temperatures. The area fraction of vapour bubbles in two-dimensional images reveals a large variation (between 0.20 and 0.34, Table 1), which reflects the uncertainty in the assumption that area fractions are approximate measures of volume fractions (Bakker and Diamond 2006; Doppler et al. 2013). All inclusions have regular and equant shapes and do not show significant variation in size on rotation. The recommended procedure of volume fraction ( $\varphi$ ) estimation of negative crystal-shaped inclusions is not feasible according to Bakker and Diamond (2006). However, a mean volume fraction that can be applied to all inclusions is estimated from a large number of investigated inclusions, their homogeneity in microthermometry and their distribution in the quartz sample. Consequently, calculated molar volumes (Table 2) illustrate a relative large variation of 23.2 to 27.9  $\text{cm}^3 \text{mol}^{-1}$ , which may not reflect true variation in densities. However, the large numbers of inclusions that are measured in *NI-002f* define an area fraction of about 0.28 as obtained from a best-fit Gaussian distribution function, which may correspond to the average volume fraction of all fluid inclusions, and a molar volume of 25.6–25.7  $\text{cm}^3 \text{mol}^{-1}$  for both groups.

The sample *NI-001a* also demonstrates a homogeneous fluid inclusion assemblage (Table 1; Fig. 2). Ice dissolution occurs at a mode of  $-7.4$  °C and clathrate dissolution at  $+5.0$  °C. These temperatures reveal only minor variation in the entire fluid inclusion assemblage. The volume fraction of the vapour bubble at room temperatures is estimated at 0.30, but displays a relative large variation of  $\pm 0.06$ . These values were obtained from a Gaussian distribution function that was fitted to the volumetric data. The centre of this curve is assumed to represent accurately the volume

fraction of the vapour phase in all fluid inclusions (c.f. average value). Subsequently, these primary data are used to calculate the composition and molar volume of each fluid inclusion (Supplementary material), with average values of 84.0 mass %  $\text{H}_2\text{O}$ , 9.2 mass %  $\text{CO}_2$ , 6.8 mass % NaCl and 26.2  $\text{cm}^3 \text{mol}^{-1}$ , respectively (Table 2). Seven inclusions in *NI-001a* display a slightly different microthermometrical behaviour (Table 1), with lower ice dissolution temperatures (around  $-9.4$  °C) and similar clathrate dissolution temperatures (around  $+4.8$  °C). These temperatures correspond to slightly higher calculated salinities (8.5 mass % NaCl).

Inclusions from the homogeneous assemblage in the sample of the third experiment (*NI-002b*) show a minor range in ice dissolution temperatures between  $-10.0$  and  $-7.6$  °C, with a mode at  $-9.2$  °C (Table 1; Fig. 2), at nearly constant clathrate dissolution temperatures (mode  $+5.2$  °C). The volume fraction of the vapour phase is estimated at about 0.31. The composition is calculated at 81.4 mass %  $\text{H}_2\text{O}$ , 10.8 mass %  $\text{CO}_2$  and 7.8 mass % NaCl, with a molar volume of 26.8  $\text{cm}^3 \text{mol}^{-1}$  (Table 2).

The thermodynamic properties of these natural fluid inclusions can be illustrated with phase diagrams in the ternary  $\text{H}_2\text{O}-\text{CO}_2-\text{NaCl}$  system. The stability field of a  $\text{CO}_2$ -clathrate (according to Bakker et al. 1996; and Bakker 1997) gives important constraints on microthermometric behaviour of these fluid inclusions (Fig. 3). The bulk fluid composition and molar volume of inclusions in experiment *NI-002f* are used to illustrate in theory the expected phase changes during microthermometry. At room temperature, these components are distributed in a  $\text{CO}_2$ -rich vapour bubble ( $\varphi^{\text{vap}} = 29$  %) and a low salinity aqueous liquid solution. At low temperatures, the phase assemblage consists of  $\text{CO}_2$ -clathrate, a low-density  $\text{CO}_2$  vapour bubble, ice and salt hydrate. The salt hydrate is the first solid phase to dissolve at the eutectic temperature of this fluid system, probably around  $-24$  °C. During further heating,  $Q_1$  conditions are reached at  $-8.0$  °C (Fig. 3) where ice completely dissolves, i.e.  $T_m(\text{ice})$ , and an aqueous liquid solution (with 2.6 mass %  $\text{CO}_2$  and 9.8 mass % NaCl) is produced with a higher salinity than the estimated bulk composition. In addition, this inclusion contains 18.2 vol%  $\text{CO}_2$ -clathrate and 26.2 vol%  $\text{CO}_2$ -rich vapour bubble. Upon further heating, clathrate continuously dissolves, liberating  $\text{CO}_2$  to the vapour phase and diluting the remaining aqueous liquid solution (black solid line in Fig. 3). The latter causes a shift to higher temperatures of the stability field of  $\text{CO}_2$ -clathrate (open arrows in Fig. 3). At the final breakdown point of  $\text{CO}_2$ -clathrate at  $+4.1$  °C, i.e.  $T_m(\text{cia})$ , the remaining aqueous liquid solution contain 5.6 mass %  $\text{CO}_2$  and 7.7 mass % NaCl in 71 vol% of the inclusion. The  $\text{CO}_2$ -rich vapour bubble has a molar volume of 519.6  $\text{cm}^3 \text{mol}^{-1}$ .  $Q_2$  conditions, i.e. coexistence of  $\text{CO}_2$

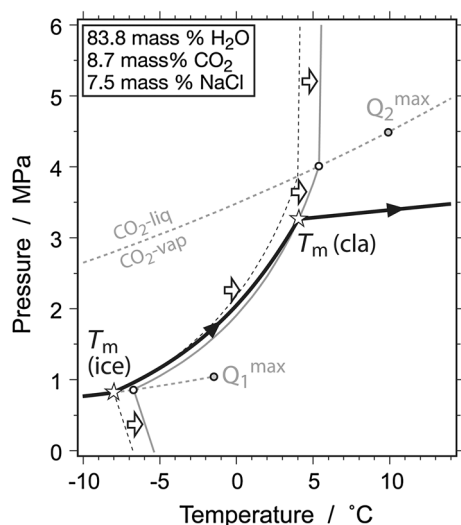


**Fig. 3** Temperature-pressure phase diagram in the system  $\text{H}_2\text{O}-\text{CO}_2$ -NaCl. The *grey solid line* represents the clathrate stability limits of the bulk fluid in inclusions with 7.5 eq. mass% NaCl. The *short dashed line* illustrates the clathrate stability limit of a relatively NaCl-enriched system at the ice dissolution temperature (8.2 eq. mass% NaCl), in the presence of a clathrate. The thick black line with reaction points  $T_m(\text{ice})$  and  $T_m(\text{cla})$  corresponds to the dissolution path of fluid inclusions with the given composition.  $Q_2^{\text{max}}$  and  $Q_1^{\text{max}}$  illustrate the maximum temperature of both quadruple points in a NaCl-free system (c.f. Bakker et al. 1996)

liquid and vapour, aqueous liquid solution and  $\text{CO}_2$ -clathrate (see Fig. 3), are not reached in these inclusions. Consequently, homogenization temperatures of  $\text{CO}_2$  liquid and vapour phase cannot be observed.

## Re-equilibration

### Experimental set-ups

Re-equilibration was performed at (1) nearly constant fluid pressure (constant- $P$  experiments;  $P_{\text{int}} = P_{\text{ext}}$ ) and (2) external fluid overpressure ( $\Delta P$  experiments;  $P_{\text{int}} < P_{\text{ext}}$ ) with pure  $\text{H}_2\text{O}$  as external fluid source. As the quartz slices are fragile, they are placed between flat distance holders

**Table 3** Pressure and fugacities of  $\text{H}_2\text{O}$ ,  $\text{CO}_2$  and NaCl in fluid inclusions at 600 °C, as calculated with the software “Loner AP”

Exp. no.	$n$	Pressure (MPa)	Fugacity (MPa)			
			$\text{H}_2\text{O}$	$\text{CO}_2$	NaCl	
NI-002f	a	30	322.2	150.0	65.2	$2.1 \times 10^{-4}$
	b	29	316.0	148.6	47.1	$2.0 \times 10^{-4}$
NI-001a	58	303.2	140.4	59.1		$1.9 \times 10^{-4}$
	7	355.4	165.8	94.1		$2.8 \times 10^{-4}$
NI-002b	58	285.3	129.7	63.8		$2.4 \times 10^{-4}$

(quartz cores with polished basal faces) to avoid disruption. All re-equilibration experiments are performed at 600 °C within the  $\alpha$ -quartz stability field at higher pressures. The internal pressure and fugacities of all the fluid components in inclusions are illustrated in Table 3, which are calculated from the average values given in Table 2.

Experiment NI-002f was performed at 309 MPa, which results in nearly constant pressure conditions of both types of fluid inclusions. The inclusions have a minor internal overpressure of 7–13 MPa at these conditions (Table 4). Inclusions were pressurized and annealed isochorically to minimize stress and monitor any pressure gradients between the fluid enclosed in the inclusions and the external fluid source. Re-equilibration was performed for 40 days, and unloading the sample was again performed along the isochoric path of the inclusions. Experiments NI-001a and NI-002b were performed at higher pressures, 394 and 398 MPa, respectively, which resulted in internal underpressures around  $-100$  MPa (Table 4). These experiments were performed for 19 and 40 days, respectively, to estimate both the type of re-equilibration processes and its time-dependency. It is expected that pressure gradients result in local deformation, such as microcracking and the formation of crystal defects adjacent to fluid inclusions.

All experiments reveal a negative gradient in  $\text{H}_2\text{O}$  fugacity, corresponding to a higher external fugacity (Table 4). According to the principles of diffusion, this gradient would provoke  $\text{H}_2\text{O}$  to move into fluid inclusions (e.g. Bakker 2009). Inclusions in experiment NI-002f have fugacity gradients of about  $-10$  MPa (between  $-9.5$  to  $-10.9$  MPa), whereas inclusions from the experiments NI-001a and NI-002b have gradients up to  $-72.5$  and  $-86.0$  MPa. Therefore, it is expected that diffusion plays a more important role in the latter experiments. In all samples, positive fugacity gradients of  $\text{CO}_2$  are induced at experimental conditions (Table 4), which should result in  $\text{CO}_2$  mass transfer out of the inclusions. The calculated fugacity of NaCl is extremely small, and, therefore, it will not be stimulated to diffuse through the quartz crystal in our experiments.

### Re-calculation of fluid composition

Changes in the bulk properties of fluid inclusions can be directly monitored by changes in  $T_m(\text{ice})$  and  $T_m(\text{cla})$ . According to the original composition and density of one fluid inclusion, a thermodynamic model can be applied to calculate the modifications of these temperatures due to diffusion processes. Within a fluid inclusion assemblage, similar calculations can be performed for all inclusions. However, the relative change in composition in each inclusion from a homogeneous assemblage corresponds to the same relative change in temperatures. Therefore, one

**Table 4** External pressure and fugacity conditions of the re-equilibration experiments (*Exp. No.*) and duration (*time*). Re-equilibration is performed at 600 °C, which results in the illustrated pressure and fugacity gradients of each component in fluid inclusions. Gradient is

Exp. no.	<i>n</i>	Time (days)	Pressure (MPa)	f(H <sub>2</sub> O) (MPa)	Pressure gradient (MPa)	Fugacity gradients (MPa)			
						H <sub>2</sub> O	CO <sub>2</sub>	NaCl	
NI-002f	a	30	40	309 ± 2	159.5 ± 1.2	+13	-9.5	65.2	2.1 × 10 <sup>-4</sup>
	b	29				+7	-10.9	47.1	2.0 × 10 <sup>-4</sup>
NI-001a	58	19	394 ± 3	212.9 ± 2.1	-91	-72.5	59.1	1.9 × 10 <sup>-4</sup>	
	7				-49	-47.1	94.1	2.8 × 10 <sup>-4</sup>	
NI-002b	58	40	398 ± 5	215.7 ± 3.5	-113	-86.0	63.8	2.4 × 10 <sup>-4</sup>	

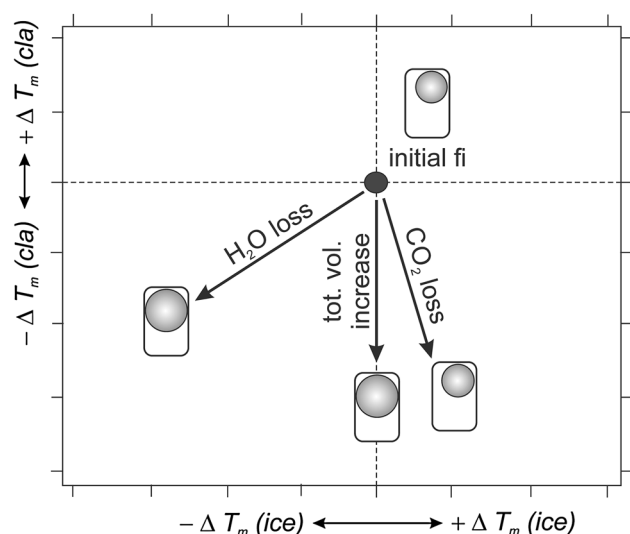


**Fig. 4** Theoretical modification of  $T_m(\text{ice})$  and  $T_m(\text{cla})$  due to H<sub>2</sub>O-loss, CO<sub>2</sub>-loss and total volume increase

inclusion can be selected from the assemblage to illustrate quantitatively the relative modifications for the whole assemblage.

One specific fluid inclusion from experiment *NI-002f* with an initial bulk composition of 83.3 mass % H<sub>2</sub>O, 9.5 mass % CO<sub>2</sub> and 7.2 mass % NaCl, and a bulk molar volume of about 26.6 cm<sup>3</sup>·mol<sup>-1</sup> was used to illustrate changes in fluid properties due to diffusion, such as the preferential loss of H<sub>2</sub>O and CO<sub>2</sub>, and due to changes in the total volume (Fig. 4). At room temperature, this original inclusion contains an aqueous liquid solution of 86.7 mass % H<sub>2</sub>O, 5.8 mass % CO<sub>2</sub> and 7.5 mass % NaCl, in addition to CO<sub>2</sub>-rich vapour bubble. The composition of the original inclusion is calculated with the program “*ICE*” (Bakker 1997) from the original ice and clathrate dissolution temperatures of -8.0 °C and +4.8 °C, respectively, with  $\varphi^{\text{vap}} = 0.31$ .

A preferential loss of 10 % of the total amount of H<sub>2</sub>O in the inclusion results in a bulk composition of 81.8

defined as internal pressure/fugacity – external pressure/fugacity. The fugacity of the external pure water is calculated from Haar et al. (1984) with the software “*Loner HGK*”

mass % H<sub>2</sub>O, 10.4 mass % CO<sub>2</sub> and 7.8 mass % NaCl, and a bulk molar volume of 29.3 cm<sup>3</sup>·mol<sup>-1</sup>. The programs “*ICE*” and “*CURVES*” (Bakker 1997) are both used to estimate numerically the new ice and clathrate dissolution temperatures at -9.0 °C and +4.2 °C, respectively. At room temperature, this inclusion contains 38 vol% CO<sub>2</sub>-rich vapour phase, with a larger molar volume of 496 cm<sup>3</sup>·mol<sup>-1</sup> compared to the original inclusion (474 cm<sup>3</sup>·mol<sup>-1</sup>), and 62 vol% aqueous liquid solution with a composition of 86.1 mass % H<sub>2</sub>O, 5.7 mass % CO<sub>2</sub> and 8.3 mass % NaCl. The trend in quantitative changes of both  $T_m(\text{ice})$  and  $T_m(\text{cla})$  has been plotted with increasing loss of H<sub>2</sub>O in Fig. 4.

The preferential loss of 10 % of the total amount of CO<sub>2</sub> in the original inclusion results in bulk composition of 84.1 mass % H<sub>2</sub>O, 8.6 mass % CO<sub>2</sub> and 7.3 mass % NaCl, and a bulk molar volume of 26.72 cm<sup>3</sup>·mol<sup>-1</sup>. This process has significant effect on the molar volume of the CO<sub>2</sub>-rich vapour bubble, which increases to 569 cm<sup>3</sup>·mol<sup>-1</sup>. The aqueous liquid solution is less affected by the loss of CO<sub>2</sub> and contains 87 mass % H<sub>2</sub>O, 5.5 mass % CO<sub>2</sub> and 7.5 mass % NaCl after diffusion. Consequently, there is only a minor change in the ice dissolution temperature towards higher temperatures, i.e. from -8.0 to -7.7 °C, whereas the clathrate dissolution temperature is more sensitive to this process and decreases from +4.8 to +3.9 °C. The volume fraction of the vapour phase remains nearly constant. These calculated changes in microthermometric properties are distinctively different from the previously calculated changes with preferential H<sub>2</sub>O diffusion (Fig. 4). Therefore, the analyses of the paired changes in  $T_m(\text{ice})$  and  $T_m(\text{cla})$ , and  $\varphi^{\text{vap}}$  provide information about the type of diffusion that has taken place during re-equilibration experiment in natural fluid inclusions.

Changes in total volume of individual fluid inclusions may occur by deformation, such as decrepitation. The formations of microcracks around fluid inclusions that do not reach the crystal surface result in a total volume increase. This does not affect the composition of the

inclusions, but results in a bulk density decrease, (i.e. an increase of the molar volume). A 10 % total volume increase of the previously illustrated fluid inclusions results in lower clathrate dissolution temperature (+3.8 °C), whereas the ice dissolution temperature is not affected (Fig. 4). Similar to preferential H<sub>2</sub>O loss, the volume fraction of the vapour phase increases to 38 vol%.

Similar to this example that calculates the effect of H<sub>2</sub>O-loss and CO<sub>2</sub>-loss, the gain of H<sub>2</sub>O and CO<sub>2</sub> results in opposite changes in ice and clathrate dissolution temperature. Consequently, comparison of ice and clathrate dissolution temperatures before and after the re-equilibration experiments gives information about the type of process that has taken place. This information cannot be obtained from a compositional diagram, in which mole fractions are displayed. The loss of CO<sub>2</sub> has the same effect on CO<sub>2</sub>/H<sub>2</sub>O ratio as the gain of H<sub>2</sub>O. The first process would result in lower clathrate dissolution temperatures and slightly higher ice dissolution temperatures, whereas the latter results in higher clathrate and ice dissolution temperatures.

In conclusion, the identification of changes in final dissolution temperatures of clathrate and ice, and changes in volume fractions of the vapour phase at room temperature allow the identification of the processes that have caused these alterations in our experiments with natural fluid inclusions.

## Results

### Morphological modifications

Inclusions from experiment *NI-002f* (constant-*P* experiment) do not show morphological alteration after re-equilibration, i.e. the relative size, elongation, diameter and morphology are unchanged (Fig. 5). Most inclusions have equant and regular shapes with straight inclusion walls that are defined by the crystallographic orientation of quartz, approaching a negative crystal shape, before and after the experiment. The area fraction of the vapour bubble in most inclusions is increased from an average value from 0.28 to 0.34 (Fig. 6a), as clearly visible in Fig. 5, whereas the dimensions of the total inclusion remain constant. Both types of fluid inclusions from this sample reveal similar changes in area fractions. A correlation between the modification in  $\varphi^{\text{vap}}$  and  $T_m$  (cla) was not observed; therefore, the increase of  $\varphi^{\text{vap}}$  is not related to a modification of total volume of the inclusions, but to the loss of fluid components by diffusion.

Inclusions exposed to  $\Delta P$  conditions for 19 days (*NI-001a*) show minor modification of their regular and equant shape (Fig. 5). The perimeter/area ratio (see definition

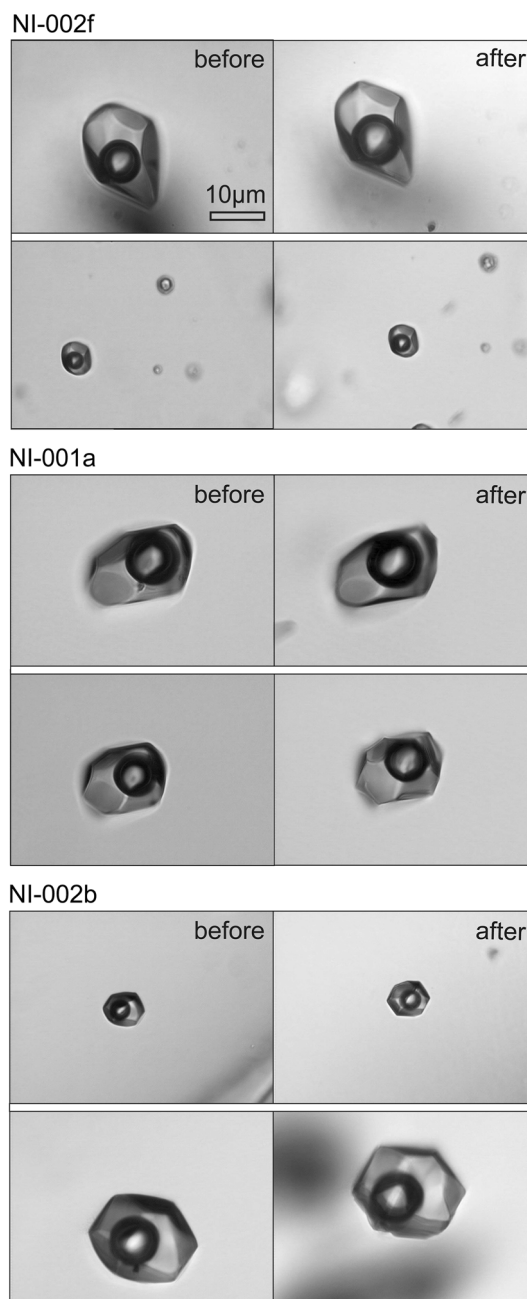


**Fig. 5** Examples of single fluid inclusions from *NI-002f* (constant *P*), *NI-001a* ( $\Delta P$ , 19 days), and *NI-002b* ( $\Delta P$ , 40 days) before and after re-equilibration experiments

Bakker and Diamond, 2006) is modified from 1.07–1.14 to 1.15–1.16 (the value 1.0 correspond to a perfect circle, increasing irregularity correspond to higher values). Fluid inclusion walls are sharpened and slightly roughened, and some are developed into concave planes, i.e. the centre of a wall plane is relatively displaced to the centre of the inclusion in comparison with the edges of this plane (c.f. skeleton quartz). These minor modifications are also observed in the 40-day  $\Delta P$  experiment *NI-002b* (Fig. 5).

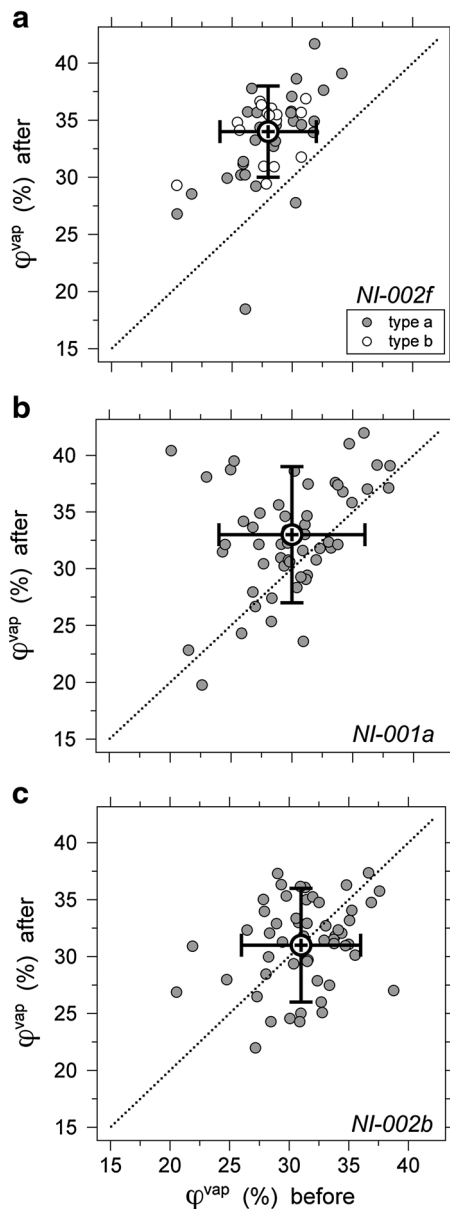


**Fig. 6** Area fractions of vapour phase in fluid inclusions illustrated as volume fraction before and after re-equilibration of **a** constant- $P$  experiment *NI-002f*, **b**  $\Delta P$  experiment *NI001a*, and **c**  $\Delta P$  experiment *NI-002b*. The symbol with error bars illustrates the centre of Gaussian distribution best-fit functions with the variability

The morphological modification does not affect all inclusions in the same extent in both  $\Delta P$  experiments. A correlation between re-equilibration time, inclusions size, their depth or any other geometrical parameter could not be determined. Both re-equilibration  $\Delta P$  experiments *NI-001a* and *NI-002b* do not show modifications in the area fractions of the vapour bubble (Fig. 6b, c, respectively); therefore, it is assumed that  $\phi^{\text{vap}}$  remain constant.

Inclusion migration has not been observed, as inclusions are found at the same relative position after re-equilibration.

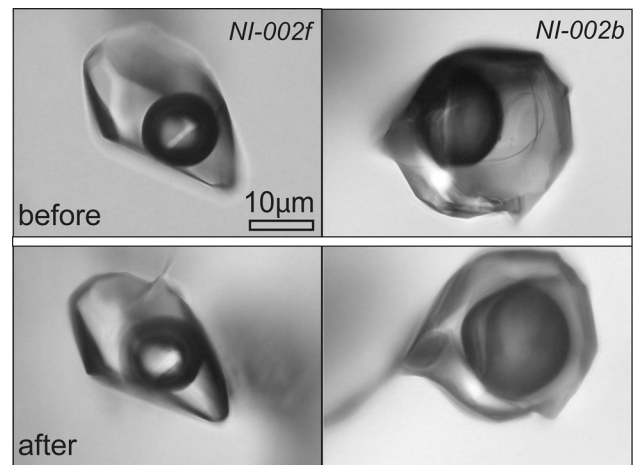


**Fig. 7** Examples of fluid inclusions from *NI-002f* and *NI-002b* that suffered from brittle deformation, i.e. the development of visible microcracks, and an anomalous increase in  $\phi^{\text{vap}}$

Few ancillary inclusions are found in all experimental set-ups that reveal leakage structures (visible microcracks) and largely increased  $\phi^{\text{vap}}$ , (Fig. 7). Some of them are totally refilled by the external fluid ( $\text{H}_2\text{O}$ ), whereas others are empty. Those inclusions are not used for further interpretation as their modification must have happened due to uncontrolled mechanical defects of the host mineral and direct fluid exchange with pore fluid along cracks.

#### Modifications of dissolution temperatures

Microthermometric measurements of inclusions from *NI-002f* after 40 days of re-equilibration under constant- $P$  conditions revealed significantly lowered clathrate dissolution temperatures after experimentation,  $\Delta T_m$  (cla) in Fig. 8a. A maximum shift of about  $-2.6\text{ }^\circ\text{C}$  to lower values was observed. On the other hand, ice dissolution temperatures remained approximately constant,  $\Delta T_m$  (ice) values in Fig. 8a. Effects of theoretically calculated  $\text{H}_2\text{O}$ -loss and  $\text{CO}_2$ -loss are also shown in Fig. 8a (c.f. Fig. 4). By excluding changes in total volume, each combination of  $T_m$  (ice) and  $T_m$  (cla) can be treated by two-dimensional vector analysis, defined by these lines of  $\text{H}_2\text{O}$  and  $\text{CO}_2$  loss. Taken into account the uncertainty in each measurement, the data lined up along the  $\text{CO}_2$ -loss axis with a small shift in the direction of  $\text{H}_2\text{O}$ -loss. Re-calculation exhibits a maximum loss of about 27 % of the amount of substance  $\text{CO}_2$  during experimentation and a maximum loss of 12 % of the amount of substance  $\text{H}_2\text{O}$ . The latter would explain the relative increase in  $\phi^{\text{vap}}$ . It should be noted that these observed modifications in dissolution temperatures are corresponding to the expected modifications according to fugacity gradients of  $\text{CO}_2$ , but in contrast to the expected  $\text{H}_2\text{O}$  diffusion into inclusions.

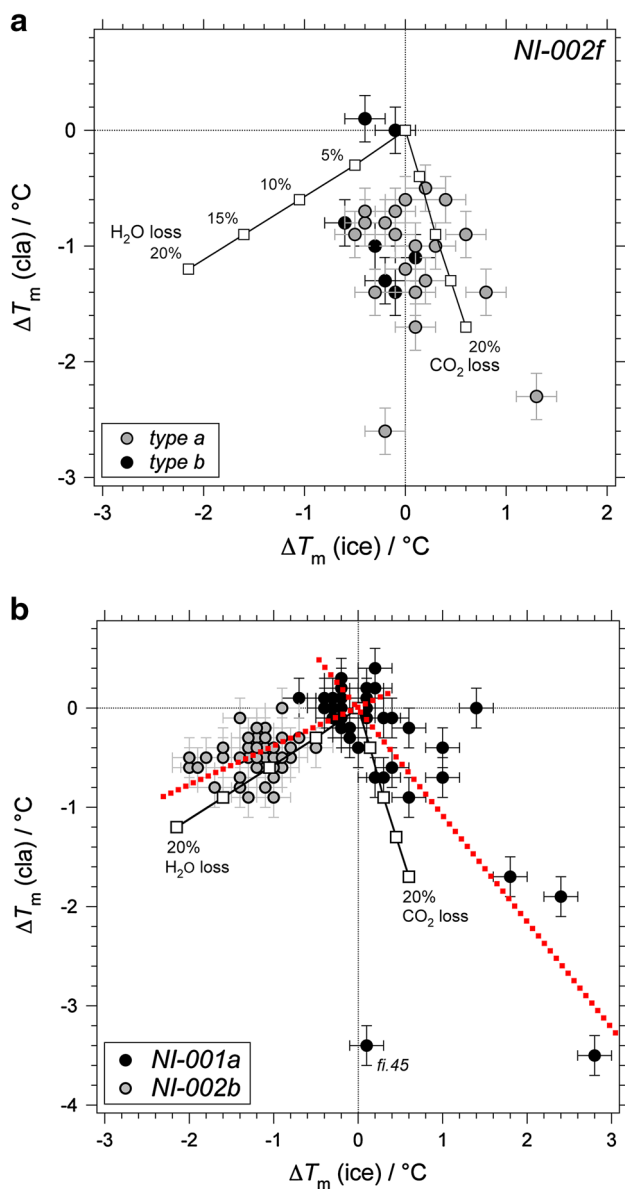


**Fig. 8** Shift of ice and clathrate dissolution temperatures, defined as temperature after minus before re-equilibration, from the experiment *NI-002f* (a), and *NI-001a*, *NI-002b* (b). The nearly straight solid lines with open squares indicate theoretically re-calculated ice and clathrate dissolution temperatures due to preferential H<sub>2</sub>O-loss (5, 10, 15, and 20 %) and CO<sub>2</sub>-loss (5, 10, 15, and 20 %). The red dashed lines in (b) are linear best-fit trends through data from the experiments *NI-001a* and *NI-002b*

Changes in dissolution temperatures of ice and clathrate in fluid inclusions after 19 days (*NI-001a*) and 40 days (*NI-002b*) of re-equilibration with pure H<sub>2</sub>O under  $\Delta P$  conditions are shown in Fig. 8b. Most inclusions from the short-time experiment *NI-001a* reveal only minor changes in these temperatures. However,  $T_m(\text{ice})$  in some inclusions increased with up to 2.8°, whereas  $T_m(\text{cla})$  decreased with maximally 3.5°. The general linear trend-line through all data (red dashed line in Fig. 8b) illustrates that inclusions

must have lost CO<sub>2</sub> and gained minor amounts of H<sub>2</sub>O, in accordance with the imposed fugacity gradients, whereas the relative size of the vapour bubble remains approximately constant. This is consistent with the observed absence of modifications in volume fractions (Fig. 6b). One inclusion illustrated in Fig. 8b (*fi.45*) exemplifies the effect of total volume increase without diffusion, probably due to local microcracking that is caused by the internal under-pressure (−72.5 MPa). This inclusion displays a clear increase in  $\varphi^{\text{vap}}$  and a decrease in  $T_m(\text{cla})$ , whereas  $T_m(\text{ice})$  remains constant (c.f. Fig. 4). The shift in both  $T_m(\text{ice})$  and  $T_m(\text{cla})$  for inclusions from  $\Delta P$  experiment *NI-002b* (long-time) is distinctively different from the short-time  $\Delta P$  experiment *NI-001a* (Fig. 8b). Data are lined up along the theoretical H<sub>2</sub>O-loss trend, consequently, fluid inclusions must have lost up to 16 % of the amount of substance H<sub>2</sub>O, whereas significant modifications in CO<sub>2</sub> content are not observed. This observation is inconsistent with expected diffusional modifications according to the imposed gradients in H<sub>2</sub>O and CO<sub>2</sub> fugacity. Local deformation mechanisms triggered by the pressure difference between inclusions and pore fluid must have inhibited or interfere with diffusion processes.

In summary, modifications in fluid composition and the mobility of H<sub>2</sub>O and CO<sub>2</sub> are illustrated with specific modifications of  $T_m(\text{ice})$  and  $T_m(\text{cla})$ . Loss of CO<sub>2</sub> is deduced from these temperatures in the constant- $P$  experiment *NI-002f*, and in the short-time  $\Delta P$  experiment *NI-001a*, according to the imposed fugacity gradients. Unexpected loss of H<sub>2</sub>O is observed in the long-time  $\Delta P$  experiment *NI-002b*, in contrast to the imposed fugacity gradient. Also the constant- $P$  experiment reveals a minor amount of H<sub>2</sub>O loss. Minor gain of H<sub>2</sub>O is observed in the short-time  $\Delta P$  experiment, according to the imposed fugacity gradient.

#### Influence of inclusion size and depth

Bulk diffusion through quartz results in specific variation in the efficiency of mass transfer, dependent on inclusion size and inclusion distance to the crystal surface (e.g. Bakker 2009; Doppler et al. 2013). In theory, if the diffusion process has not resulted in equilibrium conditions, relatively small fluid inclusions (i.e. little volume) should be stronger affected by the fluid exchange than bigger ones. In addition, fluid inclusions that are closer to the surface should be more affected by diffusion processes than deep inclusions. As illustrated in the previous paragraph, the modification in  $T_m(\text{cla})$  is a direct measure of compositional modifications. The variation of  $T_m(\text{cla})$  with inclusion depth and inclusion size for the constant- $P$  experiment *NI-002f* is illustrated in Fig. 9a, b, respectively. The data display a relative large scatter in both diagrams, which is

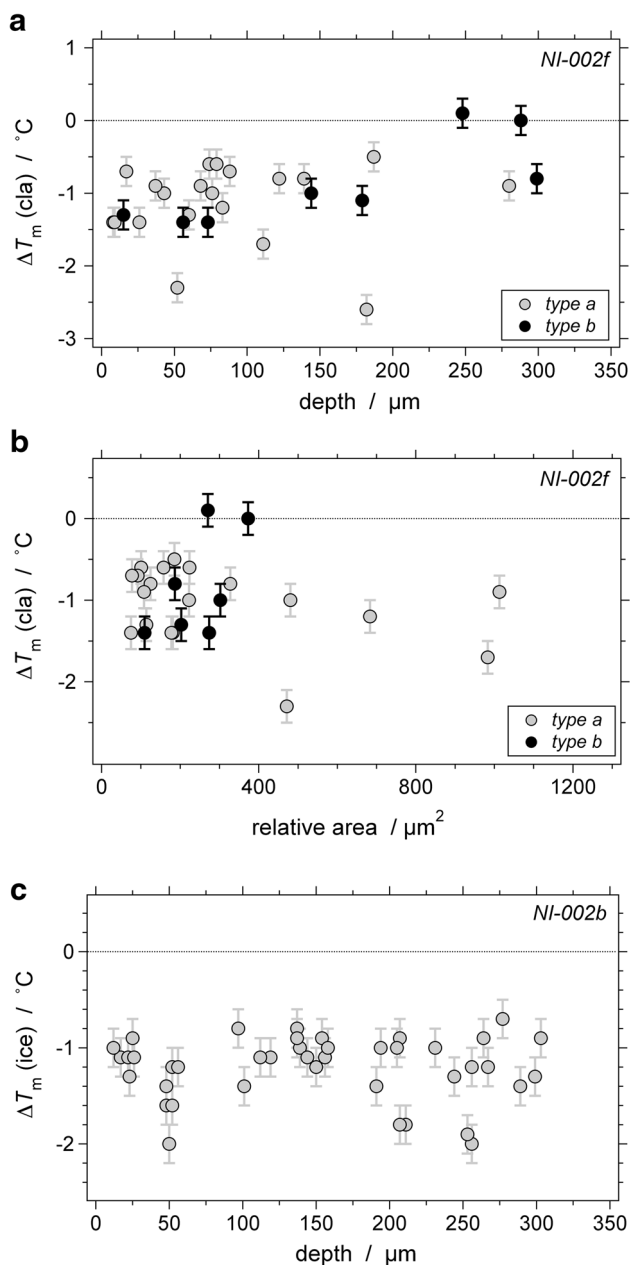


**Fig. 9** Shift in clathrate dissolution temperatures,  $\Delta T_m$  (cla), as a function of inclusion depth (a) and inclusion size (b) from constant P experiment NI-002f. c Shift in ice dissolution temperature,  $\Delta T_m$  (ice), as a function of inclusion depth from  $\Delta P$  experiment NI-002b

caused by multiple parameters that may affect  $T_m$  (cla). A minor positive trend can be observed in the depth dependency diagram (Fig. 9a), which corresponds to the expected trend by diffusion processes, although the size parameter is not taken into account in this diagram. The scatter of data in Fig. 9b can be explained by the inclusion depth parameter (Table 5): Inclusions of similar size display larger modifications at shallower depths. For example, fluid inclusions with an area of about  $100 \mu\text{m}^2$  (obtained from 2-D photomicrographs) that are closer to the surface

**Table 5** Modifications in  $\Delta T_m$  (cla) in fluid inclusion from NI-002f (type 1) of similar sizes (calculated area from photo-micrographs) as a function of inclusion depth (in  $\mu\text{m}$ ) below the quartz surface, corresponding to data illustrated in Fig. 9b

Relative size (area in $\mu\text{m}^2$ )	Depth ( $\mu\text{m}$ )	$\Delta T_m$ (cla) ( $^\circ\text{C}$ )
~100	37	-0.9
	74	-0.6
~180	8	-1.4
	26	-1.4
	187	-0.5
~220	43	-1.0
	79	-0.6
~470	53	-2.3
	76	-1.0
~980	111	-1.7
	280	-0.9

modified their  $T_m$  (cla) with  $-0.9 \text{ }^\circ\text{C}$ , whereas deeper inclusions only varied  $-0.6 \text{ }^\circ\text{C}$ . Table 5 gives examples for a variety of sizes, i.e.  $\sim 180$ ,  $\sim 220$ ,  $\sim 470$  and  $\sim 980 \mu\text{m}^2$ , with similar results. The coeval dependence of inclusion size and depth on compositional modifications illustrates that diffusion processes play an important role in the constant-P experiment NI-002f.

Fluid inclusions from the long-time  $\Delta P$  experiment NI-002b do not reveal any depth dependency on modifications (Fig. 9c). In this case, modifications in ice dissolution temperatures are selected to illustrate the influence of inclusion depth. A correlation between fluid alteration and both inclusion size and depth is not observed, and therefore, other processes such as local deformation must have played a more important role than diffusion in  $\Delta P$  experiments.

**Discussion**

Textural modifications

The conditions of the constant-P re-equilibration and  $\Delta P$  re-equilibration experiments result in only minor modification of fluid inclusion shape after 40 days at  $600 \text{ }^\circ\text{C}$  (see Fig. 5). Morphological features in the adjacent quartz crystal as a result of under-pressurized fluid inclusions, such as a halo of satellite inclusions as reported by Pecher (1981), Sterner and Bodnar (1989) and Vityk et al. (1994), have not been observed in the present study. The magnitude of “under-pressure” is, therefore, the controlling factor in the development of satellite inclusions. Fluid inclusions from the  $\Delta P$  re-equilibration experiments NI-001a and NI-002b have an under-pressure of about  $-91$  to

–113 MPa, which result in minor roughening of fluid inclusion walls, and illustrate the first signs of the development of irregular inclusions (c.f. Pecher 1981). This roughening is completely absent in the constant- $P$  experiment *NI-002f*.

#### Scattered data

The experimental conditions have been calculated from an average value of bulk composition and density of the homogeneous fluid inclusion assemblage. Figure 2 illustrates a minor variation in ice and clathrate dissolution temperatures, which correspond to a minor variation in the original properties of individual members of the assemblage. Consequently, the imposed experimental gradients in fugacity and pressure are slightly different for each individual fluid inclusion. Therefore, the modifications of  $T_m$  (ice) and  $T_m$  (cla) are slightly different for individual fluid inclusions, which result in a limited scatter of data of re-equilibrated inclusions. It would be incorrect to select just one inclusion from the assemblage and interpret re-equilibration processes without taken into account the experimental uncertainties. This uncertainty is further increased if single-fluid inclusions are effected by micro-cracks, which are not always visible by microscopy. The trend of modifications illustrated by the whole assemblage is, therefore, a proper indication of true modifications of fluid properties due to the experimental set-up.

#### Mobility of H<sub>2</sub>O and CO<sub>2</sub>

Fluid inclusions in the constant- $P$  experiment *NI-002f* illustrate primary an increase of volume fraction of the vapour phase and a decrease in  $T_m$  (cla), whereas  $T_m$  (ice) is nearly constant. The first observation may correspond to a total volume increase of fluid inclusions. However, a systematic correlation between  $T_m$  (cla) and  $\varphi^{\text{vap}}$  is absent. The reliability of  $\varphi^{\text{vap}}$  values is assumed to be much less than those of dissolution temperatures, and therefore, the correlation between  $T_m$  (ice) and  $T_m$  (cla) provides the main argument for the inferred processes. This correlation illustrates a loss of CO<sub>2</sub>, in accordance with the imposed fugacity gradient. The correlation also illustrates a minor loss of H<sub>2</sub>O, which is in conflict with the fugacity gradient, because diffusion of H<sub>2</sub>O into inclusions is expected. The increase in  $\varphi^{\text{vap}}$  is also consistent with the loss of H<sub>2</sub>O. Diffusion of H<sub>2</sub>O against fugacity gradients has already been reported by Bakker and Jansen (1990, 1994) in experiments with synthetic fluid inclusions. The mechanism of H<sub>2</sub>O loss cannot be explained by diffusion processes, and it is more likely controlled by a selective extraction of H<sub>2</sub>O into the quartz lattice due to local stress in the quartz crystal (see Hollister 1990; Bakker and Jansen 1994; Bakker 2009). Thereby H<sub>2</sub>O

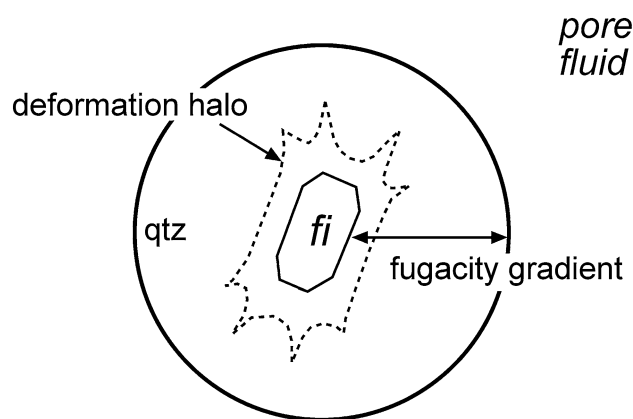


**Fig. 10** Schematic illustration of the two driving forces of fluid inclusion modifications in quartz at high temperatures: 1. deformation, that is restricted to a small zone around the inclusions, and 2. fugacity gradients

is transported from the inclusions to the grain boundary by mobile crystal defects that remain active as long as there is stress on the host quartz. The fluid inclusions in constant- $P$  experiment have a slight over-pressure, and therefore, local deformation of inclusion walls may take place, resulting in the loss of H<sub>2</sub>O. Apparently, diffusion of H<sub>2</sub>O according to fugacity gradients is inhibited by this deformation halo (Fig. 10). In other words, defect structures are more efficient in attracting H<sub>2</sub>O molecules than the supply of H<sub>2</sub>O molecules by diffusion.

Fluid inclusions from the short-time (19 days)  $\Delta P$  experiment *NI-001a* behave according to the imposed fugacity gradients: loss in CO<sub>2</sub> and minor gain in H<sub>2</sub>O. However, the long-time (40 days)  $\Delta P$  experiment *NI-002b* reveals a completely different behaviour of fluid inclusions. This experiment illustrates only the loss of H<sub>2</sub>O, whereas CO<sub>2</sub> is more or less immobile. The major difference between both experiments is that the internal under-pressure is higher in *NI-002b* than in *NI-001a* (–113 vs. –91 MPa). It is assumed that this difference is the main cause for this contrasting behaviour, in addition to experimentation time. The development of a larger deformation halo around fluid inclusions and the possibility of recovery must have resulted in solely the loss of H<sub>2</sub>O.

The general model of the behaviour of fluid inclusions in all experiments is illustrated in Fig. 10. Two processes are of major importance for the modification of fluids inclusions: 1. diffusion; and 2. deformation. Both processes are in direct competition at high temperatures and pressures. Deformation adjacent to fluid inclusions is caused by both internal over- and under-pressures. The deformed quartz is able to absorb fluid components from inclusions in defect structures, mainly H<sub>2</sub>O but CO<sub>2</sub> can also be included. Therefore, fluid components are always lost from the inclusions if deformation processes take place. The

deformation halo can only contain a limited amount of fluid components, unless this halo reaches the surface of the grain. Recovery of the quartz crystal around fluid inclusion would release fluid components to the inclusions or pore space. Probably, CO<sub>2</sub> is more sensitive to this recovery process than H<sub>2</sub>O. Bulk diffusion of fluid components through quartz is a process that may take place under constant pressure as well as differential pressure conditions at high temperatures (e.g. Doppler et al. 2013). The efficiency of diffusion is dependent on the properties of the quartz crystal. The development of deformation structures, which are already saturated with H<sub>2</sub>O and CO<sub>2</sub> from inclusions, may inhibit bulk diffusion from the pore fluid into fluid inclusions, but enhance pipe diffusion along crystal defects (Bakker and Jansen 1990).

The discussed deformation processes are independent from general rock deformation processes, which result from specific regional stress conditions. This has been experimentally tested by Tarantola et al. (2010) and Diamond et al. (2010) with similar type of natural fluid inclusions. They have also observed the preferential loss of H<sub>2</sub>O from fluid inclusions, as already described by Bakker and Jansen (1990, 1994). However, modification processes that are observed in this study cannot be excluded in these deformation experiments. The experimental loss of H<sub>2</sub>O from fluid inclusions can also be obtained in a stress-less situation.

### Geological interpretation

The properties of fluid inclusions cannot be fully interpreted in terms of geological environments if knowledge about the possibilities of post-entrapment alterations is incomplete. Natural fluid inclusion assemblages may contain a micro-themometrical diversity and a variety of volume fraction of the vapour phase. This assemblage may contain information about post-entrapment modification, if a systematic trend in dissolution temperatures of clathrate and ice is observed. In addition, trends in CO<sub>2</sub> homogenization temperatures and volume fractions may also be used to identify re-equilibration processes. Any systematic association of these temperatures and volume fractions can be interpreted as specific re-equilibration processes and provides reconstruction possibilities of original trapping conditions.

### Conclusions

Natural H<sub>2</sub>O–CO<sub>2</sub>–NaCl-rich fluid inclusion can be affected by diffusion and deformation processes in hydrothermal experimental studies at 600 °C and pressure between 300 and 400 MPa. Modifications in ice dissolution temperatures, clathrate dissolution temperatures and volume

fractions of the vapour phase can be used to identify individually processes such as preferential H<sub>2</sub>O loss, preferential CO<sub>2</sub> loss and total volume change. In nearly constant pressure experiments (minor pressure difference between inclusion and pore fluid), fugacity gradients promote the diffusion of CO<sub>2</sub> out of inclusions. The minor loss of H<sub>2</sub>O is not consistent with the applied fugacity gradient, but may result from deformation of inclusion walls according to minor pressure differences. CO<sub>2</sub>-loss and gain of H<sub>2</sub>O are according to fugacity gradients in the short-term  $\Delta P$  experiments (internal under-pressure). However, fugacity gradients play only a minor role in the mobility of fluid components in the long-term  $\Delta P$  experiment. Deformation halos around fluid inclusions in the longer-term experiment inhibit diffusion according to these gradients. These inclusions reveal only the loss of H<sub>2</sub>O, in contrast to the expected gain according to these gradients. Modifications in fluid composition and density may occur in inclusions without any optical evidence or textural alterations.

**Acknowledgments** This research is funded by the Austrian Science Fund (FWF); project number: P22446-N21. Alfons van den Kerkhof, Matthew Steele-MacInnis and an anonymous reviewer are thanked for their advice and comments that greatly improved the quality of this manuscript.

### References

- Anderko A, Pitzer KS (1993) Equation of state representation of phase equilibria and volumetric properties of the system NaCl–H<sub>2</sub>O above 573 K. *Geochim Cosmochim Acta* 57:1657–1680
- Audetà A, Günther D (1999) Mobility and H<sub>2</sub>O loss from fluid inclusions in natural quartz crystals. *Contr Mineral Petrol* 137(1–2):1–14
- Ayllon F, Bakker RJ, Warr LN (2003) Re-equilibration of fluid inclusions in diagenetic-anchizonal rocks of the Cinerá-Matallana coal basin (NW Spain). *Geofluids* 3:49–68
- Bakker RJ (1997) Clathrates: computer programs to calculate fluid inclusion V–X properties using clathrate melting temperatures. *Comput Geosci* 23:1–18
- Bakker RJ (2003) Package FLUIDS 1. Computer programs for analysis of fluid inclusion data and modelling bulk fluid properties. *Chem. Geol.* 194:3–23
- Bakker RJ (2009) Re-equilibration of fluid inclusions: bulk diffusion. *Lithos* 112:277–288
- Bakker RJ, Diamond LW (2006) Estimation of volume fractions of liquid and vapour phases in fluid inclusions and definition of inclusion shape. *Am Mineral* 91:635–657
- Bakker RJ, Jansen JBH (1990) Preferential water leakage from fluid inclusions by means of mobile dislocations. *Nature* 345:58–60
- Bakker RJ, Jansen JBH (1994) A mechanism for preferential H<sub>2</sub>O leakage from fluid inclusions in quartz, based on TEM observations. *Contr Mineral Petrol* 116:7–20
- Bakker RJ, Dubessy J, Cathelineau M (1996) Improvement in clathrate modelling: I. The H<sub>2</sub>O–CO<sub>2</sub> system with various salts. *Geochim Cosmochim Acta* 60:1657–1681

- Barker AJ (1995) Post-entrapment modification of fluid inclusions due to overpressure: evidence from natural samples. *J metamorphic Geol* 13:737–750
- Baumgartner M, Bakker RJ (2010) Raman spectra of ice and salt hydrates in synthetic fluid inclusions. *Chem Geol* 275:58–66
- Chueh PL, Prausnitz JM (1967) Vapor-liquid equilibria at high pressures. Vapor-phase fugacity coefficients in nonpolar and quantum gas mixtures. *Ind Eng Chem Fundam* 6:492–498
- Diamond L, Tarantola A, Stünitz H (2010) Modification of fluid inclusions in quartz by deviatoric stress I: experimentally induced changes in inclusion shape and microstructures. *Contr Mineral Petrol* 160:825–843
- Doppler G, Bakker RJ (2014) The influence of the  $\beta$ -phase transition of quartz on fluid inclusions during re-equilibration experiments. *Lithos* 198–199:14–23
- Doppler G, Bakker RJ, Baumgartner M (2013) Fluid inclusion modification by H<sub>2</sub>O and D<sub>2</sub>O diffusion: the influence of inclusion depth, size, and shape in re-equilibration experiments. *Contr Mineral Petrol* 165:1259–1274
- Duan Z, Moller N, Weare JH (1995) Equation of state for the NaCl-H<sub>2</sub>O-CO<sub>2</sub> system: prediction of phase equilibria and volumetric properties. *Geochim Cosmochim Acta* 59:2869–2882
- Faleiros AM, Cruz Campanha GA, Faleiros FM, Silveira Bello RM (2014) Fluid regimes, fault-valve behavior and formation of gold-quartz veins—The Morro do Ouro mine, Ribeira Belt, Brazil. *Ore Geol Rev* 56:442–456
- Ferrero S, Bodnar RJ, Cesare B, Viti C (2011) Re-equilibration of primary fluid inclusions in peritectic garnet from metapelitic enclaves, El Hoyazo, Spain. *Lithos* 124:117–131
- Haar L, Gallagher JS, Kell GS (1984) NBS/NRC steam tables
- Hollister LS (1990) enrichment of CO<sub>2</sub> in fluid inclusions in quartz by removal of H<sub>2</sub>O during crystal-plastic deformation. *J Structural Geol* 12:895–901
- Krenn K, Bauer C, Proyer A, Mpsokos E, Hoinkes G (2008) Fluid entrapment and reequilibration during subduction and exhumation: a case study from the high grade Nestos shear zone, Central Rhodope, Greece. *Lithos* 104:33–53
- Pecher A (1981) Experimental decrepitation and re-equilibration of fluid inclusions in synthetic quartz. *Tectonophysics* 78:567–583
- Ridley J, Hagemann SG (1999) Interpretation of post-entrapment fluid inclusion re-equilibration at the Three Mile Hill, Marvel Loch and Griffins Find high-temperature lode-gold deposits, Yilgarn Craton, Western Australia. *Chem Geol* 154:257–278
- Schwab RG, Freisleben B (1988) Fluid CO<sub>2</sub> inclusion in olivine and pyroxene and their behaviour under high pressure and temperature conditions. *Bull Mineral* 111:297–306
- Sterner SM, Bodnar RJ (1989) Synthetic fluid inclusions—VII. Re-equilibration of fluid inclusions in quartz during laboratory-simulated metamorphic burial and uplift. *J Metamorph Geol* 7:243–260
- Sterner SM, Hall DL, Keppler H (1995) Compositional re-equilibration of fluid inclusions in quartz. *Contr Mineral Petrol* 119:1–15
- Tarantola A, Diamond L, Stünitz H (2010) Modification of fluid inclusions in quartz by deviatoric stress II: experimentally induced changes in inclusion volume and composition. *Contr Mineral Petrol* 160:845–864
- Vityk MO, Bodnar RJ (1995) Textural evolution of synthetic fluid inclusions in quartz during reequilibration, with applications to tectonic reconstruction. *Contr Mineral Petrol* 121:309–323
- Vityk MO, Bodnar RJ (1998) Statistical microthermometry of synthetic fluid inclusions in quartz during decompression re-equilibration. *Contr Mineral Petrol* 132:149–162
- Vityk MO, Bodnar RJ, Schmidt CS (1994) fluid inclusions as tectonothermobarometers: relations between pressure-temperature history and reequilibration morphology during crustal thickening. *Geology* 22:731–734
- Vityk MO, Bodnar RJ, Dubok IV (1995) Natural and synthetic re-equilibration textures of fluid inclusions in quartz (Marmarosh Diamonds): evidence for refilling under conditions of compressive loading. *Eur J Mineral* 7:1071–1087
- Wilkins RWT, Barkas JP (1978) Fluid inclusions, deformation and recrystallization in granite tectonites. *Contr Mineral Petrol* 65:293–299